

ON THE APPLICABILITY ASSESSMENT OF VON KARMAN'S MOMENTUM THEORY IN PREDICTING THE WATER-ENTER LOAD OF V-SHAPED BODY

Yujin LU^{1, 2}, Alessandro Del Buono², Tianhang Xiao¹, Alessandro Iafrati² & Jinfa XU¹

¹Nanjing University of Aeronautics and Astronautics, Nanjing, 210016, People's Republic of China

²National Research Council-Institute of Marine Engineering (CNR-INM), Rome, 00128, Italy

Abstract

The water landing motion of an amphibious aircraft is a complicated problem, that can lead to uncomfortable riding situation and structural damage due to large vertical accelerations followed by sorts of dynamic responses. The problem is here investigated by solving unsteady incompressible Reynolds-averaged Navier-Stokes equations enclosed by the standard $k-\omega$ turbulence model. The theoretical solutions established by the momentum theory are also employed. In order to validate the relationships between initial vertical velocity and peak value of vertical acceleration, a free fall test case of 2D symmetric wedge oblique entry is presented first. Then, the quantitative relations are investigated to water landing event of a 3D cabin section extracting from an amphibious aircraft. Detailed results through the free surface and pressure distribution are provided to show the slamming effects, and their physical implications are discussed. The result shows that a linear function of maximal acceleration to the square of initial vertical velocity can be built up for all cases, contributing to variation prediction of acceleration.

Keywords: water landing, amphibious aircraft, free fall, maximal acceleration, linear function

1. Introduction

Amphibious aircraft is a special flight vehicle that is capable to take off and land on water and conventional runways [1]. Recently, the amphibious aircrafts have drawn considerable attentions by the nations with maritime supremacy due to their potential military and civilian applications. During the flight operational envelop of amphibious aircraft, the hydrodynamic impact load during landing on water is regarded as the most dangerous phase which significantly influences the survivability and structure tolerance [2]. However, for the full model of an amphibious aircraft with such complicated geometry, it is tough to make series of experimental tests in the real sea condition which incur tremendous cost of time, manpower and even more currency, occasionally with low accuracy causing by the experimental apparatus. In order to clearly examine the load characteristics exerting on the aircraft, the most straightforward and available way is to perform scaled-model experiments in water tunnels. For instance, NACA Langley Memorial Aeronautical Laboratory has conducted comprehensive experimental studies on the water-entry problems, resulting extensive and valuable archived test data and recommendations in industrial applications [3], presenting the effects upon performance of changes in design parameters such as dead rise angle, depth of step, configuration of hull body, hydrofoils, etc., and which are still pivoting for numerical validation and seaplane design. In the field of ocean engineering, water tank has always seemed as the primary choice through the scaled model to evaluate the kinematic characteristics. Whereas, for the seaplane which has hull body and wing components, the similarity for hydrodynamic and aerodynamic are quite different [4]. Froude number Fr is used to guarantee the correct reproduction of the ratio between inertia and gravitational forces, while Reynolds number Re accounting for viscous effects is not properly scaled [5,6].

Meanwhile, with the recent increasingly development of computational fluid dynamics (CFD) methods, it is now capable of simulating the motion of amphibious aircraft in full scale instead of the time-consuming experimental methods. Many researchers have focused on different phases during the whole process, such as takeoff/landing, skiing, and other serious situations. For the takeoff process, Qiu et al. [1] proposed a decoupled algorithm to investigate the kinematic characteristics, which compute the aerodynamic forces based on the full configuration and hydrodynamic forces from hull body separately. The whole process was divided into a number of small time-step, and the forces were calculated at each time step. Porpoising motion, as an unstable oscillation phenomenon that threatens the flying safety of amphibious aircrafts, was evaluated by Duan et al. [4] using a two-phase flow solver in OpenFOAM. Both slipstream caused by the propeller and external forces, viz. thrust and elevator forces, were taken into consideration as well. Results highlighted hydrodynamic force plays an important role on the heaving and pitching oscillations, while the aerodynamic force only plays an auxiliary role. Similar to the water landing scenarios of amphibian aircraft, ditching events of conventional aircrafts share the same fluid mechanisms and phenomena, and have been numerically studied more by many researchers. The effects of initial ditching stage [7-10], structural damage [2,11,12], wave conditions [13,14] and various numerical strategies [15-17] on modelling the kinematic characteristics and fluid phenomena are mostly paid attention. Nevertheless, the vertical acceleration is more significant, which causes mental problems for the crews and can lead to structural damages for the fuselage once it strikes the water [18]. Thus, it deserves more attention amid the load characteristics of an amphibian/aircraft landing on water, particularly on the peak.

Speaking of the ditching, water impact is one phase of it, the most important one in terms of complex fluid-structure interaction. The phases of ditching are: approach, impact, landing, and flotation [11]. Von Karman [19] first proposed an analytical estimation method based on a wedge-shaped water impact and introduced the method to settle the impact loads on seaplanes. Subsequently, a number of researches related to water impact have been documented through theoretical and experimental ways [20-26]. It has been shown that, during the slamming stage which is the first stage of a free fall motion entering water, the structure experiences a rapid change of vertical acceleration, which is similar with early stage of landing characteristics [27]. Alternatively, a few researchers investigated the relationship between the maximum acceleration and initial parameters on free-fall water entry. Among these studies, Gong et al. [28] simulated a series of cases with various initial entering velocity of the wedge based on Smoothed Particle Hydrodynamics (SPH) model, and relations for the maximum force on the wedge and the corresponding time in terms of the initial entering velocity of the wedge have been directly expressed by fitting formulas considering limited Froude number. In the work of Abraham et al [29], the drag-coefficient results were found to be independent of some investigated quantities, such as the sphere velocity, surface tension, flow regime and Reynolds number. Then, the algebraic representations of drag coefficient have been established by two fitted polynomials with respect to the dimensionless depths. Effects of parametric variation, such as impact velocity, radius, and mass of the sphere on the impact force and the acceleration, have also been discussed by Yu et al [30]. The peak value of the non-dimensional impact force has been found independent of the velocity and the radius, except the mass of sphere. Meanwhile, simplified expressions for the maximal force and the acceleration have been obtained through fitting the relations between the peak value of the non-dimensional force and the non-dimensional mass. The relationships have also been mentioned by other researchers' work [6, 31-34]. However, it also should be noted that only fitting functions about force and acceleration were discussed in the previous studies, and the detailed theoretical basis with related relationships and applications are still not well documented yet.

The present study is dedicated to implementing numerical analysis on a two-dimensional symmetric wedge and a three-dimensional cabin section with free fall water entry in order to investigate and build up kinds of relations on parameters, based on the transformation of conservation of momentum theory, such as maximal acceleration and the corresponding velocity. Particular attention is given to investigating the effects of horizontal velocity, and three-dimensional effect on the relationships. Furthermore, the relation is expected to be utilized to predict the load performance of amphibian water landing scenarios. The present work outlines as follows. Section 2 presents the methodology for the theoretical and numerical approaches, together with the detailed models and computational setup. The main results are reported and discussed in Sec. 3 with conclusions drawn in Sec. 4.

2. Methodology and Computational Setup

2.1 Von Karman's Theoretical Method and Transformation

Pioneer research in water-entry problem has been conducted by von Karman [19], based on momentum theorem and the added mass for the force prediction as the V-shaped body penetrates the water surface. The theorem of momentum equation for predicting hydrodynamic load of water entry can be concluded during the impacting, that is,

$$Mv_0 = (M + m_{\text{added}}) \cdot v(t) \quad (1)$$

where M is the mass of the wedge, v_0 is the initial vertical velocity before the impact, $v(t)$ is the instantaneous velocity during impacting and m_{added} , namely added mass briefly computed by $m_{\text{added}} = (\pi\rho r^2(t))/2$ (see Figure 1), using the flat-plate approximation of the added mass. It is assumed the mass of a half disk of water of radius $r(t)$ is moving with the wedge [35], ignoring the effect of water pile-up. By this way, the velocity of the body can be formulated by:

$$v(t) = \frac{v_0}{1 + \frac{\pi\rho z^2(t)}{2M \tan^2(\beta)}} \quad (2)$$

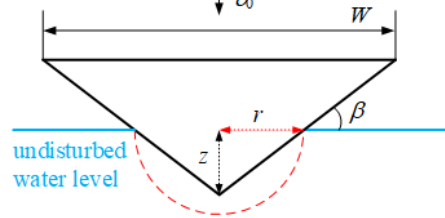


Figure 1 - Von Karman's momentum approach.

Then, differentiating (2), it is easy to compute the acceleration as followed [36]:

$$a(t) = \frac{\pi\rho z(t)}{Mv_0 \tan^2(\beta)} \cdot v^3(t) \quad (3)$$

and the impact acceleration reaches its peak as:

$$a_{\text{max}} = v_0^2 \left(\frac{5}{6}\right)^3 \frac{1}{g \cdot \tan(\beta)} \sqrt{\frac{2\pi\rho}{5M}} \quad (4)$$

Note that a_{max} is a non-dimensional value. It is interesting to notice that a_{max} is proportional to v_0^2 , implying that the initial vertical velocity performs a significant role on the variation of acceleration. In addition, most of researchers have focused on the empirical or estimation formula for the impacting force. In the present study, we aim at predicting the forces based on the formula by several results from experiment or simulation.

2.2 Numerical Method

The unsteady incompressible Reynolds-averaged Navier-Stokes equations enclosed by the standard $k-\omega$ two-equation turbulence model are solved by the finite volume method in the present study. The Semi-Implicit Pressure Linked Equations (SIMPLE) algorithm is applied to achieve an implicit coupling between pressure and velocity, and the gradient is reconstructed with the Green-Gauss Node Based method. The modified High Resolution Interface Capturing (HRIC) scheme is adopted to volume fraction discretization. The convection terms, as well as diffusion terms, are turned into algebraic parameters using second-order upwind and second-order central methods, respectively. The unsteady terms are discretized in the time domain by applying a second-order implicit scheme.

Volume of fluid (VOF) scheme, first proposed by Hirt and Nichols [37], is applied in the present computational scheme to capture the water-air interface by introducing a variable called the volume fraction of the water in the computational cell, shown by α_w , which varies between 0 (air) and 1 (water), defined as:

$$\alpha_w = V_w/V, \quad (5)$$

where V_w is the volume of water in the cell and V is the volume of the cell. The volume fractions of

two phases in a cell must sum up to one:

$$\alpha_w + \alpha_a = 1. \quad (6)$$

The effective term φ_m of any physical properties, such as density, viscosity, etc., of the mixture of water and air in the transport equations is determined by:

$$\varphi_m = \varphi_w \alpha_w + \varphi_a (1 - \alpha_w). \quad (7)$$

To accurately capture the dynamic behavior as well as the load characteristics of water landing process, the motion of the body in response to the fluid forces and moments at the surface is determined using a six degree-of-freedom (6DOF) model. The 6DOF model solves the equations for the rotation and translation of the center of mass of the object. The equation for the translation in the global inertial coordinate system is formulated as:

$$m \frac{dv}{dt} = \mathbf{F}, \quad (8)$$

and the rotation of the object is solved in the body local coordinate system by:

$$\mathbf{L} \frac{d\boldsymbol{\omega}}{dt} + \boldsymbol{\omega} \times \mathbf{L}\boldsymbol{\omega} = \mathbf{M}. \quad (9)$$

Subsequently, a dynamic mesh strategy, which moves the entire fluid mesh rigidly along with the object at each time step in relation to the solution of the six-degree-freedom model, is employed to deal with the relative motion between the fluid and the rigid body. As neither mesh distortion nor mesh reconstruction happens, the high quality of the initial mesh remains unchanged during the whole simulation, and thus, the solution accuracy of both flow field and water-air interface capture was not degraded for such unsteady problems with large relative motion. It should be mentioned that the water surface level should keep stationary regardless of the translation or rotation of the mesh. To achieve this goal, the function of α_w needs to be implemented on the boundary condition where the water volume fraction of each grid cell was assigned according to its global inertial coordinates. Specifically, the figure is one for the cells located below the interface, and zero for the cells above.

2.3 Models and Computational Setup

The relation shown in the formula (4) will be discussed in the motion of oblique entry of a symmetric wedge firstly. Oblique water impact, as the motion of the body is similar with that of amphibious aircraft landing on water, it can be seen as the simplified model to study the effect of varying vertical velocity on the load characteristics, as well as the variation of horizontal velocity. In the work of Russo et al.[38], the asymmetric and oblique impact have been studied by systematically varying the heel angle θ and velocity angle α . Only the vertical and horizontal motions are allowed for the wedge in this experiment. The wedge has width $W=20$ cm and deadrise angle $\beta =37^\circ$ in the experiment, however, the heel angle is ignored herein seen in Figure 2. To simulate a relative two-dimensional motion, the cell number in the y-direction is set to 1, and the cell size in the present study is 0.002 m. Figure 3 shows the mesh topology and grid density with two zoom-in views. The length of the square boundary is 10 times the width of this wedge. The computational domain was constructed with structured quadrilateral grids and the minimum size of mesh is 0.05 cm. The right hand and bottom sides were set as velocity inlet, when the boundary condition of pressure outlet was specified on the top and the left sides (see Figure 3).

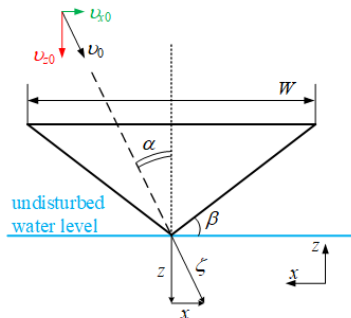


Figure 2 - Sketch of the wedge at the onset of the entry along with relevant geometric and dynamic parameters.

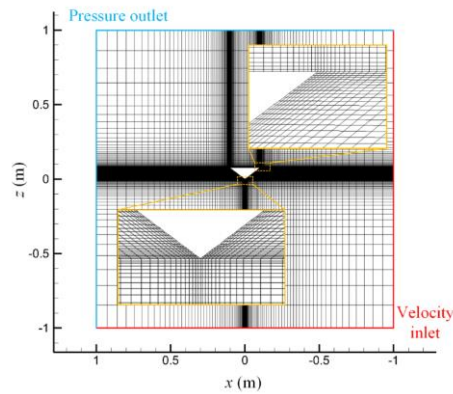


Figure 3 - Grid topology and density of wedge.

As a second step of test, a cabin section, a part of the seaplane, is dissected numerically to examine the three-dimensional effect on the relation, referring to Eq. (4). The geometry parameters of the cabin section are shown in Figure 4 with length $L=1.61$ m, width $W=3.27$ m, deadrise $\beta=30^\circ$ and mass $M=600$ kg. The section is manually lifted to the desired height and released for freely fall in the experiment [39]. The real tank is 5 m in depth and 60 m in length and width. While, in the simulation, as depicted in Figure 5, the cabin is initially released near the water surface with different initial impact velocity to study the effect of velocity on the acceleration. Figure 5 shows the boundary conditions and the initial relative pressure field on the left side boundary. A dashed red cuboid was created surrounding the cabin with refined meshes to capture the water surface more precisely.

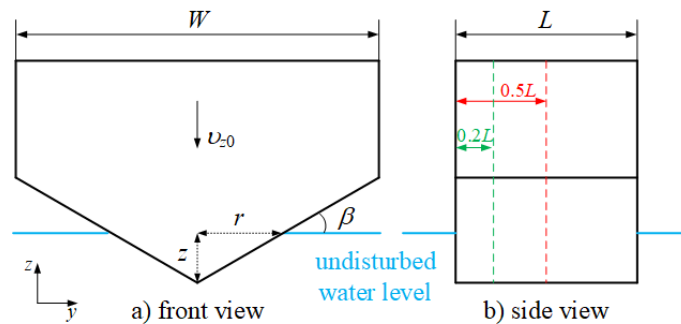


Figure 4 - Sketch of the cabin section along with relevant geometric parameters.

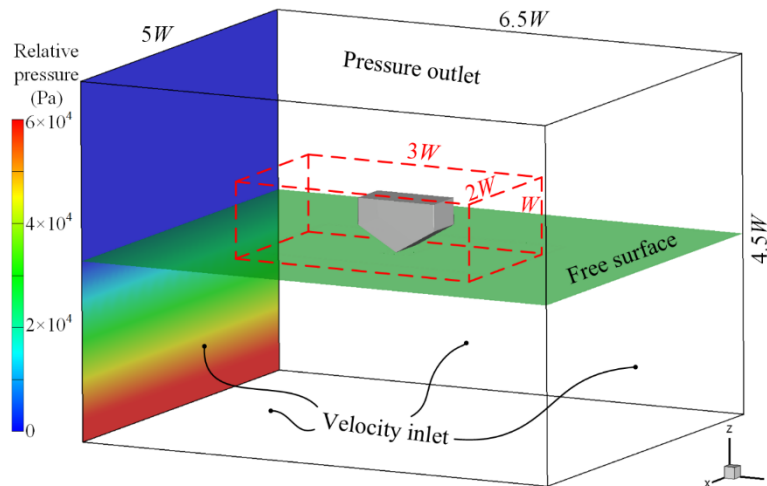


Figure 5 - Boundary conditions and the initial flow field.

3. Results and Discussion

3.1 2D Symmetric Wedge

3.1.1 Effect of Vertical Velocity

First, the accuracy and efficiency of the numerical method have been validated by a symmetric

On the applicability assessment of Von Karman's momentum theory in predicting loads

wedge. At $t=0$ s, the wedge is dropped against calm water, entering the free surface with an initial resultant velocity 2.75 m/s and velocity angle $\alpha = 20^\circ$. Figure 6 shows the comparison between present study and experimental data [38] in terms of the normalized resultant displacement and acceleration. As can be seen, the results are in good agreement with experiments, though a little discrepancy occurs on the acceleration. Thus, the solutions for the wedge are obtained which compares favorably with experimental data with satisfactory accuracy.

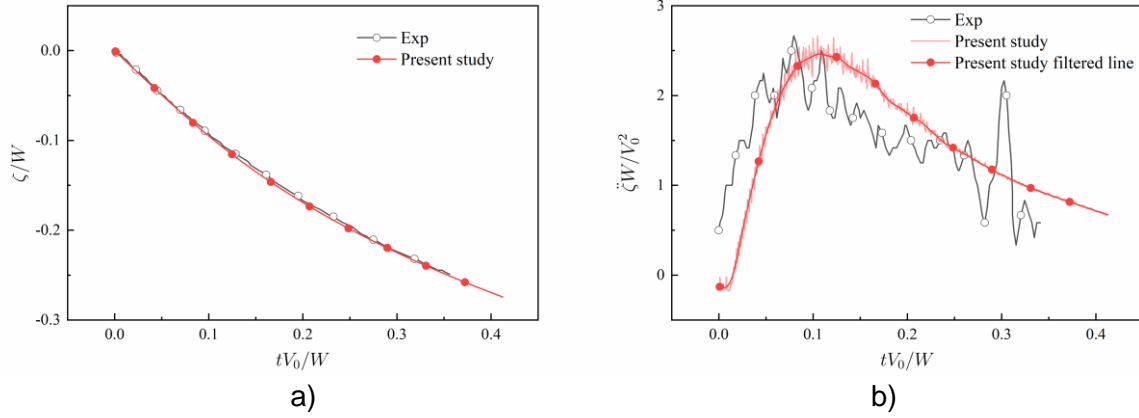


Figure 6 - Comparison of present study and experimental data: a) normalized resultant displacement; b) normalized resultant acceleration.

Subsequently, for understanding the effect of the variation of vertical velocity, the case of $\alpha = 20^\circ$ is regarded as the reference case, where v_{x0} remains unchanged. In comparison, α varies from 10° to 50° in 10° increments, implying a decrease of vertical velocity. The time histories of a_z , defined as $a_z = (F_w + F_a - mg)/g$, are depicted in Figure 7a), along with several pink crosses marking the maximum value a_{zmax} . It indicates that constant v_{x0} and systematically increasing α causes a significant reduction in a_z due to the corresponding decline in the v_{z0} . Note that the positive values of a_z point to the opposite direction of gravity. Particularly, as v_{z0} drops to a certain point, a_z will experience a moderating trend in proximity to zero, stating it 'smooth entry' [40]. The analysis of a_{zmax} and v_{z0} , presented in Figure 7b), plots the solution of a_{zmax} as a linear function of v_{z0}^2 , supporting the relationship formulated in the Eq. (4). Moreover, the other two series of simulations have been conducted by changing the constant value of v_{x0} , as depicted in Figure 8, where all data are identically on a straight line. As evidenced in Table 1, we are cheerful to appreciate that the linear relation between a_{zmax} and v_{z0}^2 exists, and only a small deviation could be observed in the slope k compared with the theoretical one. However, there is an intercept value of b among the numerical results. On the other hand, it reveals the significant contribution of the vertical component of the velocity to the linear relation, regardless of the value of v_{x0} .

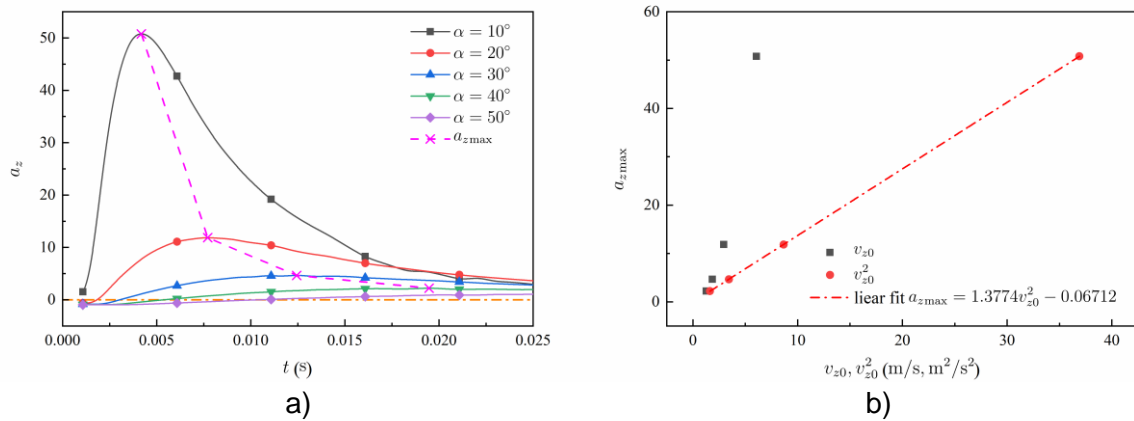


Figure 7 - Variation of acceleration z: a) versus time; b) versus initial vertical velocity.

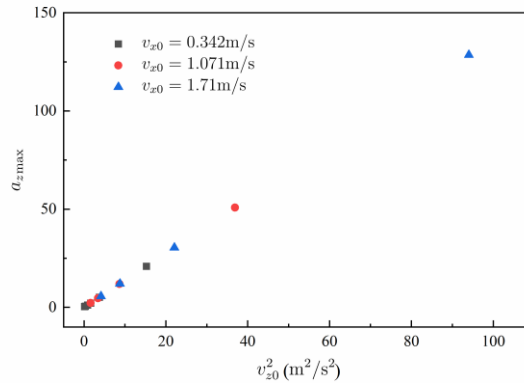


Figure 8 - Effect of the horizontal velocity on the relation between a_{zmax} and v_{z0}^2 .

Table 1 Comparison of theoretical value and present study

	a_{zmax}		
	k	err, %	b
Theoretical value	1.2807	-	-
$v_{x0}=0.342$ m/s	1.3594	6.14	0.0026
$v_{x0}=1.071$ m/s	1.3774	7.54	-0.067
$v_{x0}=1.710$ m/s	1.3655	6.62	0.0897

3.1.2 Effect of horizontal velocity

In the previous section, we have discussed the effect of initial vertical velocity on the load characteristics for oblique entry of wedge, and naturally it is meaningful to check the role of initial horizontal velocity played on these relations. By making v_{z0} constant and altering α to vary v_{x0} , similar to the operation in the former section, Figure 9 presents the time histories of a_x and a_z exerted on the wedge at various velocity angle α , referring to the first case of $\alpha = 20^\circ$. As can be seen, the value of a_x shows an obvious decreasing trend when reducing α upon water impact, whereas no apparent alterations could be found in a_z , significantly differing from the situations of varying initial vertical velocity. Therefore, the data of a_{xmax} are extracted and compare with three different formations of v_{x0} as illustrated in Figure 10. It is cheerful to appreciate a linear function can be fitted, although the function is established between a_{xmax} and v_{x0} , instead of v_{x0}^2 , which is remarkably different from cases of varying v_{z0} . Moreover, the pressure contour plots around the wedge with variable α , when a_{xmax} is achieved, are illustrated in the upper side of Figure 11, where pressure coefficient C_p is defined as $C_p = (p - p_0) / [0.5\rho(v_{z0}^2 + v_{x0}^2)]$, and the value of v_{x0} is referring to the initial horizontal velocity in the case of $\alpha = 40^\circ$. As can be seen, a higher-pressure region occurs at the right-hand side of the wedge, while a negative zone on the left, leading to the variation of a_x . It is therein evidenced that the pressure field varies significantly in the range $\alpha = [10, 40]$. The comparison of the upper and lower side in Figure 11, it evidences that the water jets originate from the pressure peak that, in turn, is located at the intersection between the air-water interface and the wedge, and the low-pressure zone is close to the kneel which would cause a rotation once the tilting motion is released.

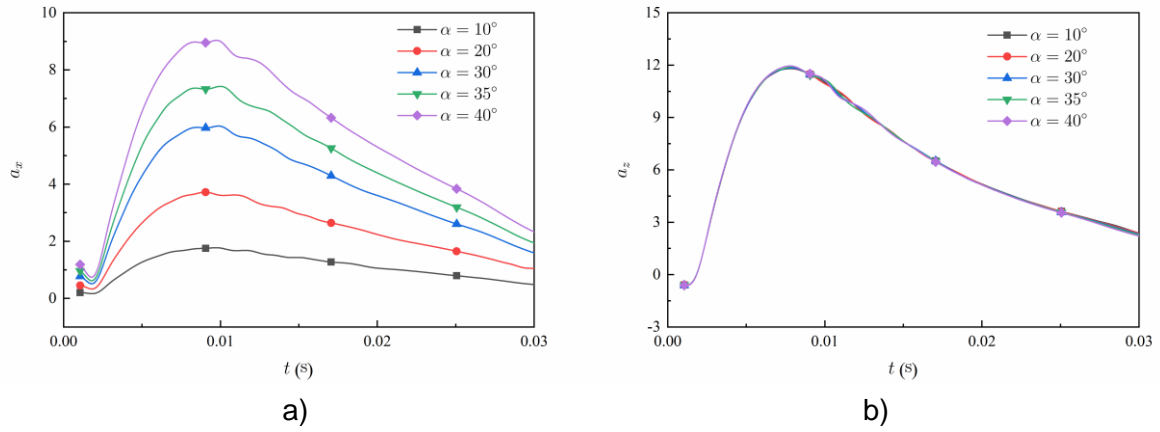


Figure 9 - Time histories of acceleration with different inclined angles: a) a_x ; b) a_z .

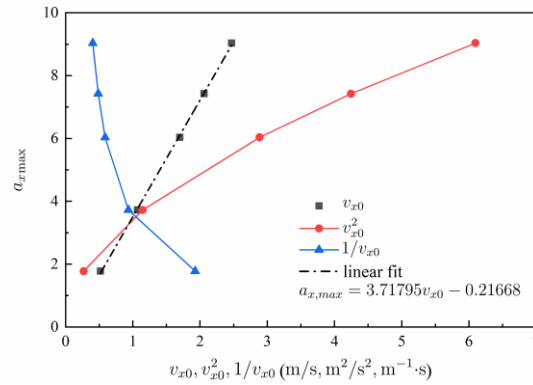


Figure 10 - Variation of maximum acceleration x versus initial horizontal velocity.

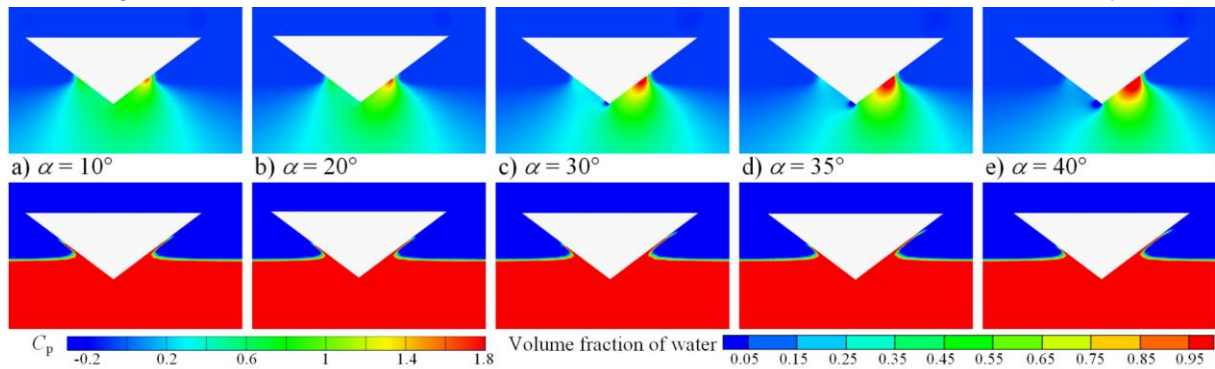


Figure 11 - Pressure distribution and water volume fraction for different velocity angle α when a_x reaches its maximum.

3.2 A Cabin Section in 3D

Thanks to the tests previously presented, it has been proved that it is possible to evaluate the load characteristics with the help of the linear relations, demonstrated in Eq. (4), with large initial vertical velocity. This section presents the results of our computational simulations of the cabin section, (see Figure 4), entering the free surface with various initial vertical velocity v_{z0} . Eleven cases with a series of v_{z0} from 0.5 m/s to 6 m/s are simulated. Figure 12a) shows the evolution of a_z acting on the cabin during the water entry. Moreover, the results have been filtered with a cutoff frequency 62.5 Hz. At the beginning of the impacting, the overall acceleration is less than zero indicating that gravity force plays the dominant role, while the hydrodynamic force only plays an auxiliary role at the onset of entry. As the body is submerging, a_z becomes greater than zero and reaches its peak value subsequently, which means the hydrodynamic force occupies a significant position during this event. Obviously, a_z is linked with the initial impact velocity. The smaller v_{z0} is, the more moderate the variation tendency of a_z will be presented until there is no clear peak. This behaviour can be also observed in Figure 12b), where pressure coefficient $C_p = (p - p_0)/(0.5\rho v_{z0}^2)$ is exacted along the

On the applicability assessment of Von Karman's momentum theory in predicting loads

section at $0.5L$ with v_{z0} chosen as 6 m/s. As the initial impact velocity increases, the overall values of C_p become higher together with three extreme values for each case. One is at $y=0$, the apex of the body, so-called stagnation point, where the flow velocity is almost equal to zero, and the others peak at the grey region. It can be seen that the distance between the peak points becomes narrow, and the difference is less pronounced as v_{z0} grows, which means the penetrating motion tends to be stable gradually.

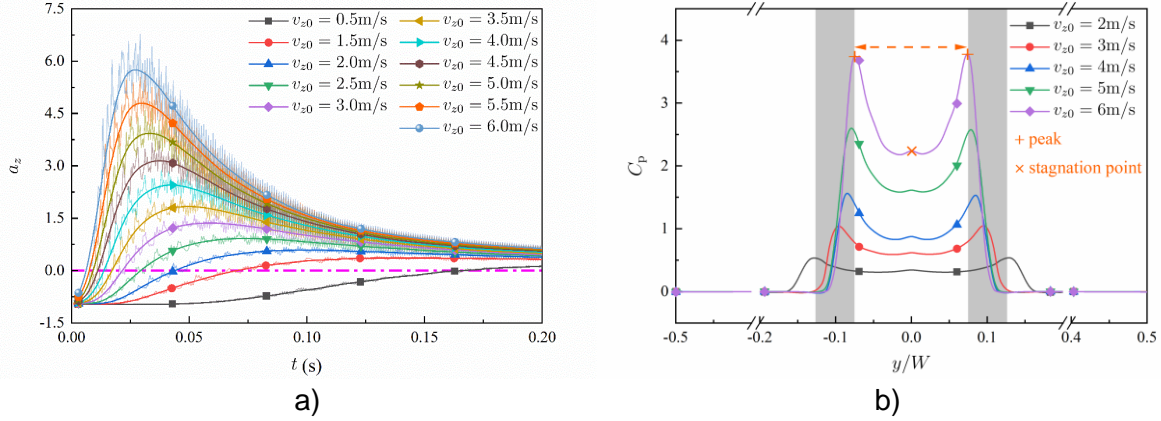


Figure 12 - a) Time histories of acceleration z a_z with different initial vertical velocity v_{z0} ; b) pressure coefficient at $0.5L$ with different v_{z0} .

Figure 13a) demonstrates $a_{z\max}$ is still a linear function to v_{z0}^2 , fitted by $a_{z\max} = 0.1605v_{z0}^2 - 0.0744$, where k is slightly greater than the theoretical one with 8.66% error, listed in Table 2. Figure 13b) shows the results of C_p at three distinctive cross-sections, viz., $0.1L$, $0.2L$ and $0.5L$, with the change of v_{z0} , where the deviation δ obviously exists that may contribute to the difference between the numerical and the theoretical solution. It is clear to see that the value of δ becomes larger as v_{z0} rises, indicating more significantly the three-dimensional effect performs. Till now, we can see that the linear relationship between the maximum value of acceleration and the square of initial velocity has also been built up, along with a small deviation compared to the result of Eq. (4).

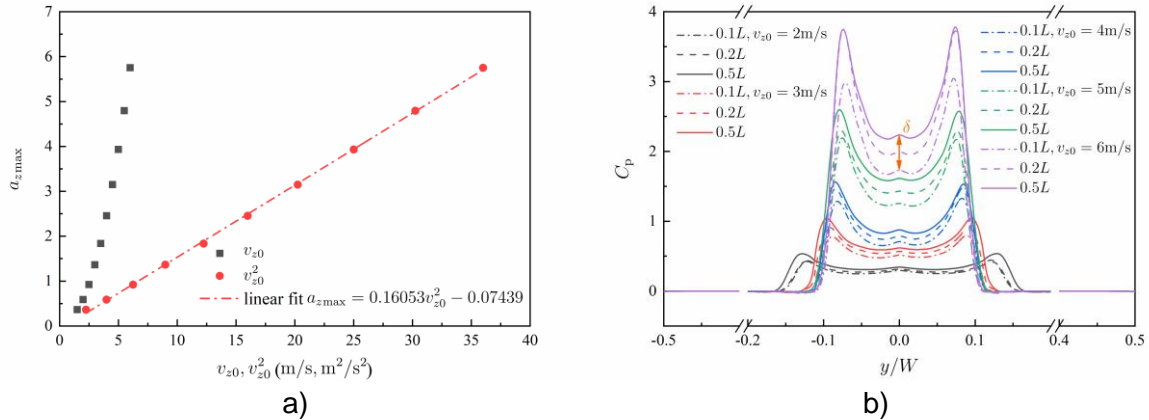


Figure 13 - a) Variation of $a_{z\max}$ versus v_{z0} and v_{z0}^2 ; b) pressure coefficient at three distinctive cross-sections for different v_{z0} .

Table 2 Comparison of theoretical data and present study

	$a_{z\max}$		
	k	err, %	b
Theoretical value	0.1477	-	-
Present study	0.1605	8.66	-0.0744

4. Conclusion

In the present study, we numerically investigated the load characteristics of two models, such as a 2D symmetric wedge water entry and a 3D cabin section water entry, where the effect of initial vertical velocity on the maximum acceleration is comprehensively evaluated. The main contribution and

On the applicability assessment of Von Karman's momentum theory in predicting loads

results are summarized, which can be drawn as:

- 1) For the V-shaped sectional area of body impacting on water surface, the maximum vertical acceleration increases with the initial vertical velocity, and it is widely to acknowledge herein that the value of maximal acceleration is proportional to the square of the initial velocity. Besides, the horizontal velocity and three-dimensional effect have no significant influence on the linear function.
- 2) Additionally, for oblique entry, the various horizontal velocities associated with maximal acceleration have also been investigated. It is meaningful to appreciate the maximum horizontal acceleration is a linear function of initial horizontal velocity itself, rather than the square value.
- 3) The water landing of V-shaped hull on amphibious aircraft is expected to test the ability of the quantitative relation obtained from the theoretical formula for engineering application, predicting the maximal overload.

5. Acknowledgements

This work has been supported by China Scholarship Council (CSC, No. 202106830092) and the Project TORPEDO (inTerazione fluidO stRuttura in ProBlEmi Di impattO) cooperated in the Institute of Marine Engineering of the National Research Council of Italy.

6. Contact Author Email Address

Mail to: xthang@nuaa.edu.cn

7. Copyright Statement

The authors confirm that they hold copyright on all of the original material included in this paper. The authors also confirm that they have obtained permission, from the copyright holder of any third party material included in this paper, to publish it as part of their paper. The authors confirm that they give permission, or have obtained permission from the copyright holder of this paper, for the publication and distribution of this paper as part of the ICAS proceedings or as individual off-prints from the proceedings.

References

- [1] Qiu L and Song W. Efficient decoupled hydrodynamic and aerodynamic analysis of amphibious aircraft water takeoff process. *Journal of Aircraft*, Vol. 50, No. 5, pp.1369-1379, 2013.
- [2] Hughes K, Vignjevic R, Campbell J, Vuyst T D, Djordjevic N and Papagiannis L. From aerospace to offshore: bridging the numerical simulation gaps-simulation advancements for fluid structure interaction problems. *International Journal of Impact Engineering*, Vol. 61, Nov, pp. 48-63, 2013.
- [3] Benson J M, and Bidwell J M. Bibliography and review of information relating to the hydrodynamics of seaplanes. NACA ACR-L5G28, 1945.
- [4] Duan X, Sun W, Chen C, Wei Meng, and Yang Y. Numerical investigation of the porpoising motion of a seaplane planing on water with high speeds. *Aerospace Science and Technology*, Vol. 84, Jan, pp. 980-994, 2019.
- [5] Terziev M, Tezdogan T, and Incecik A. Scale effects and full-scale ship hydrodynamics: a review. *Ocean Engineering*, Vol. 245, Feb, pp. 110496, 2022.
- [6] Iafrati A, and Grizzi S. Cavitation and ventilation modalities during ditching. *Physics of Fluids*, Vol. 31, No. 5, pp. 052101, 2019.
- [7] Xiao T, Lu Z, and Deng S. Effect of Initial Pitching Angle on Helicopter Ditching Characteristics Using SPH Method. *Journal of Aircraft*, Vol. 58, No. 1, pp. 167–181, 2021.
- [8] Guo B, Liu P, Qu Q and Wang J. Effect of Pitch Angle on Initial Stage of a Transport Airplane Ditching. *Chinese Journal of Aeronautics*, Vol. 26, No. 1, pp. 17-26, 2013.
- [9] Qu Q, Liu C, Liu P, Guo B and Agarwal R K. Numerical Simulation of Water-Landing Performance of a Regional Aircraft. *Journal of Aircraft*, Vol. 53, No. 6, pp. 1680–1689, 2016.
- [10]Zheng Y, Qu Q, Liu P, Wen X and Zhang Z. Numerical Analysis of the Porpoising Motion of a Blended Wing Body Aircraft during Ditching. *Aerospace Science and Technology*, Vol. 119, Dec, pp. 10731, 2021.
- [11]Siemann M H, Schwinn D B, Scherer J and Kohlgruber D. Advances in Numerical Ditching Simulation of Flexible Aircraft Models. *International Journal of Crashworthiness*, Vol. 23, No. 2, pp. 236-251, 2017.
- [12]Yang X, Ma J, Wen D and Yang J. Crashworthy design and energy absorption mechanisms for helicopter structures: a systematic literature review. *Progress in Aerospace Sciences*, Vol. 114, Apr, pp. 100618, 2020.
- [13]Woodgate M A, Barakos G N, Scrase N and Neville T. Simulation of helicopter ditching using smoothed particle hydrodynamics. *Aerospace Science and Technology*, Vol. 85, Feb, pp. 277–292, 2019.
- [14]Xiao T, Lu Y, Deng S, Zhi H, Zhu Z and Chen J. Hydrodynamic characteristics of a helicopter ditching on different positions of wavy water. *Journal of Aircraft*, Vol. 58, No. 5, pp. 1-12, 2021.
- [15]Bisagni C and Pigazzini M S. Modelling strategies for numerical simulation of aircraft ditching. *International Journal of Crashworthiness*, Vol. 23, No. 4, pp. 377-394, 2017.
- [16]Siemann M N and Langrand B. Coupled fluid-structure computational methods for aircraft ditching simulation: comparison of ALE-FE and SPH-FE approaches. *Computers and Structures*, Vol. 188, Aug, pp. 95–108, 2017.
- [17]Xiao T, Qin N, Lu Z, Sun X, Tong M and Wang Z. Development of a smoothed particle hydrodynamics method and its application to aircraft ditching simulations. *Aerospace Science and Technology*, Vol. 166, July, pp. 28-43, 2017.
- [18]Neuberg O and Drimer N. Fatigue limit state design of fast boats. *Marine Structures*, Vol. 55, Sep, pp. 17-36, 2017.
- [19]von Karman T. The impact on seaplane floats during landing. NACA TN-321, 1929.
- [20]Zhao R and Faltinsen O M. Water entry of two-dimensional bodies. *Journal of Fluid Mechanics*, Vol. 246, Jan, pp. 593-612, 1993.
- [21]Scolan Y M and Korobkin A A. Three-dimensional theory of water impact. part 1. inverse wagner problem. *Journal of Fluid Mechanics*, Vol. 440, Aug, pp. 293-326, 2001.
- [22]Korobkin A. Analytical models of water impact. *European Journal of Applied Mathematics*, Vol. 15, No. 6, pp. 821-838, 2004.
- [23]Korobkin A A and Scolan Y M. Three-dimensional theory of water impact. part 2. linearized wagner problem. *Journal of Fluid Mechanics*, Vol. 549, Feb, pp. 343-373, 2006.
- [24]Wu G X and Sun S L. Similarity solution for oblique water entry of an expanding paraboloid, *Journal of Fluid Mechanics*, Vol. 745, April, pp. 398-408, 2014.
- [25]Breton T, Tassin A and Jacques N. Experimental investigation of the water entry and/or exit of axisymmetric bodies. *Journal of Fluid Mechanics*, Vol. 901, Oct, pp. A37, 2020.
- [26]Zekri H J, Korobkin A A and Cooker M J. Gravity effect on water entry during an early stage. *Journal of Fluid Mechanics*, Vol. 916, June, pp. A10, 2021.
- [27]Wang J, Lugni C and Faltinsen O M. Experimental and numerical investigation of a freefall wedge vertically entering the water surface. *Applied Ocean Research*, Vol. 51, June, pp. 181-203, 2015.

On the applicability assessment of Von Karman's momentum theory in predicting loads

- [28]Gong K, Liu H and Wang B. Water entry of a wedge based on SPH model with an improved boundary treatment. *Journal of Hydrodynamics*, Vol. 21, No. 6, pp. 750-757, 2009.
- [29]Abraham J, Gorman J, Reseghetti F, Sparrow E, Stark J and Shepard T. Modeling and numerical simulation of the forces acting on a sphere during early-water entry. *Ocean Engineering*, Vol. 76, Jan, pp. 1-9, 2014.
- [30]Yu P, Shen C, Zhen C, Tang H and Wang T. Parametric study on the free-fall water entry of a sphere by using the RANS method. *Journal of Marine Science and Engineering*, Vol. 7, No. 5, pp. 122, 2019.
- [31]Iafrati A. Experimental investigation of the water entry of a rectangular plate at high horizontal velocity. *Journal of Fluid Mechanics*, Vol. 799, June, pp. 637-672, 2016.
- [32]Wen X, Liu P, Qu Q and Hu T. Impact of wedge bodies on wedge-shaped water surface with varying speed. *Journal of Fluids and Structures*, Vol. 92, Jan, pp. 102831, 2020.
- [33]Wang S, Gadelho J, Islam H and Soares C G. CFD modelling and grid uncertainty analysis of the free-falling water entry of 2D rigid bodies. *Applied Ocean Research*, Vol. 115, Oct, pp. 102813, 2021.
- [34]Sheng C, Yu P, Wang T and Chen N. A CFD based kriging model for predicting the impact force on the sphere bottom during the early-water entry. *Ocean Engineering*, Vol. 243, Jan, pp. 110304, 2022.
- [35]Mei X, Liu Y and Yue D K P. On the water impact of general two-dimensional sections. *Applied Ocean Research*, Vol. 21, Feb, pp. 1-15, 1999.
- [36]Panciroli R, Abrate S and Minak G. Dynamic response of flexible wedges entering the water. *Composite Structures*, Vol. 99, May, pp. 163-171, 2013.
- [37]Hirt C W and Nichols B D. Volume of fluid (VOF) method for the dynamics of free boundaries. *Journal of Computational Physics*, Vol. 39, No. 1, pp. 201-225, 1981.
- [38]Russo S, Jalalisendi M, Falcucci G and Porfiri M. Experimental characterization of oblique and asymmetric water entry. *Experimental Thermal and Fluid Science*, Vol. 92, Apr, pp. 141-161, 2018.
- [39]Chen J, Xiao T, Wu B, Wang F and Tong M. Numerical study of wave effect on water entry of a three-dimensional symmetric wedge. *Ocean Engineering*, 2022. (to be published)
- [40]Vincent L, Xiao T, Yohann D, Jung S and Kanso E. Dynamics of water entry. *Journal of Fluid Mechanics*, Vol. 846, July, pp. 508-535, 2018.